HUNGARIAN JOURNAL OF
INDUSTRY AND CHEMISTRY
Vol. 51(2) pp. 21–26 (2023)
hjic.mk.uni-pannon.hu
DOI: 10.33927/hjic-2023-14

INFLUENCE OF TIC ON DENSITY AND MICROSTRUCTURE OF AL_2O_3 CERAMICS DOPED WITH NB_2O_5 AND LIF

PEDRO HENRIQUE POUBEL MENDONÇA DA SILVEIRA[1]* AND ALAELSON VIEIRA GOMES[1]

1 Department of Materials Science, Military Institute of Engineering-IME, Praça General Tibúrcio, 80, Urca, Rio de Janeiro 22290-270, BRAZIL

Ceramic matrix composites are widely studied in the ballistic sector due to their high hardness, fracture toughness, and improved ballistic performance in multilayer shielding systems. However, the presence of dopants in ceramics can pose challenges during processing and potentially compromise the final properties of the sintered material. This study focused on the ceramic processing of Al_2O_3-based ceramic matrix composites by adding 4 wt.% Nb_2O_5 (niobium oxide), 0.5 wt.% LiF (lithium fluoride), and 38.5 wt.% TiC (titanium carbide). The composites were produced using cold uniaxial pressing and conventional sintering at 1400 °C for 3 h. The composites were characterized using Archimedes' principle and scanning electron microscopy (SEM). The results revealed that the samples to which TiC was added exhibited low initial densities, indicating that the applied pressure of 50 MPa during cold pressing was insufficient to adequately densify the green bodies. Moreover, the presence of TiC led to a significant reduction in densification, making it challenging to apply a conductive coating for SEM analysis. Adjustments to the intensity of the electron beam were necessary to conduct the analysis successfully. Conversely, the samples to which TiC was not added exhibited high density values in the green state and yielded consistent results after sintering in line with previous research, indicating a satisfactory degree of sintering in the absence of TiC. These findings highlight the importance of carefully considering the addition of TiC in ceramic matrix composites during processing, which can have a significant impact on densification and subsequent material properties. The results contribute to the understanding of processing parameters with regard to the production of ceramic composites with desirable characteristics for ballistic applications.

Keywords: absence of ceramic matrix composites, Al_2O_3, Nb_2O_5, LiF, TiC, SEM, Archimedes' principle

1. Introduction

The demand for composite materials has grown due to their advantageous properties, e.g. high strength-to-weight ratio, elevated resistance and relatively low density compared to other classes of materials. For this reason, composites have been widely adopted in, for example, the aerospace, automotive and military sectors amongst various other fields in recent decades [1]-[2]. One of the main applications of composites is in ballistic protection, where these materials play a crucial role in the military field. Due to their low weight, composites are preferred when manufacturing aircraft, tanks, and bulletproof vests [3]-[6].

The ceramic materials used in ballistic armor must be able to fragment the bullet, reducing its velocity and splitting it into small fragments, which are absorbed by the rear layer of the armor composed of a flexible material capable of supporting the ceramic. Therefore, it is crucial that the ceramic material exhibits a high modulus of elasticity, as well as high hardness and good fracture toughness [7]-[10].

The main commercially used ceramic materials in the development of ballistic armor are Al_2O_3, B_4C, SiC and ceramic matrix composites (CMCs), such as the Al_2O_3-ZrO_2 or Al_2O_3-Nb_2O_5-LiF systems. However, the high cost associated with processing restrictions and the difficulties in predicting the ballistic performance of these ceramic materials impede ceramic mechanisms, making it necessary to include other elements to improve their properties and reduce costs [11]-[14].

In this regard, Al_2O_3 exhibits the best benefit-cost ratio among advanced ceramics, with high modulus of elasticity, good refractory performance, high degree of hardness, and relatively lower cost. However, due to its low fracture toughness and flexural strength, the ballistic performance of alumina is inferior to that of SiC and B_4C [15]-[17].

An important factor to be considered in the processing of ceramics for ballistic armor is the formation of a liquid phase, which enables higher densification of the material accompanied by reduced sintering temperatures without property loss. An example of this is the use of Nb_2O_5, which, when added to alumina

Received: 4 July 2023; Revised: 3 Aug 2023;
Accepted: 7 Aug 2023
*Correspondence: pedroo.poubel@gmail.com

Table 1: Density of the raw materials of the produced ceramics

Material	Density (g/cm^3)
Al_2O_3	3.98
Nb_2O_5	4.60
LiF	2.60
TiC	4.93
PEG 300	-

in quantities of 1 to 8 wt.%, provides a considerable reduction in the sintering temperature [18]-[19].

Another crucial factor is the addition of carbide to the ceramic matrix. The inclusion of ceramics, such as NbC, SiC as well as B_4C in the Al_2O_3 matrix enhances the hardness and fracture toughness [20]. Regarding the development of CMCs in armor, TiC is a material with good properties which is used as an interstitial addition to increase hardness and fracture toughness [20]-[23]. TiC is an extremely hard ceramic (Mohs hardness scale 9.0-9.5) and has a very high melting point (3260 °C) [24]. However, concerning the processing of Al_2O_3, TiC CMCs are challenging as they require techniques such as spark plasma sintering (SPS) or hot pressing (HP), which are difficult to implement. Although these techniques facilitate faster sintering with densities around 95% of theoretical values, their availability is limited [25].

With the aim simplifying processing and making it more cost-effective, this work aims to process Al_2O_3 matrix CMCs by adding TiC using conventional sintering and cold uniaxial pressing as well as sintering additives such as Nb_2O_5 and LiF.

2. Materials and methods

2.1. Raw materials

The powders used to manufacture the ceramic bodies were acquired from different sources. The α-Al_2O_3 was obtained from Treibacher Schleifmittel (Brazil) with an average grain size of 3 μm. The Nb_2O_5 was acquired from Companhia Brasileira de Metalurgia e Mineração (Brazil). The LiF used was purchased from VETEC (Brazil). The TiC applied as an additive was produced by Sigma-Aldrich (USA). The organic binder used to strengthen the green body is Polyethylene Glycol (PEG 300) manufactured by Isofar (Brazil). In *Table 1*, the compounds used to produce the ceramic compounds are presented along with their densities.

The densities of the mixtures (ρ) were determined using the Rule of Mixtures as described in *Equation 1*:

$$\rho = (m_a \cdot \rho_a) + (m_b \cdot \rho_b) \quad (1)$$

The densities of each element in the mixture (ρ_a, ρ_b) and their weight fractions (m_a, m_b) were taken into account, except for PEG which was eliminated during sintering.

The weight percentages of each element added were 0.5 of LiF, 4 of Nb_2O_5, and 38.5 wt.% of TiC. The densities of each mixture are shown in *Table 2*.

Table 2: Theoretical density of each sample mixture

Sample mixture	Density (g/cm^3)
Al_2O_3-Nb_2O_5	3.98
Al_2O_3-Nb_2O_5-LiF	3.99
Al_2O_3-TiC-Nb_2O_5	4.37
Al_2O_3-TiC-Nb_2O_5-LiF	4.37

2.2. Ceramic processing

The starting materials were placed in an alumina-coated jar. To facilitate homogenization, deionized water along with alumina balls to enhance powder comminution were added in a ratio of 1:1. Grinding and mixing were carried out in a ball mill over 8 hours before being dried in an oven at 80 °C for 48 hours.

After drying, the resulting ground mixture was deagglomerated using a pestle and mortar before being sieved to obtain the desired particle size. A sieve shaker was applied for 3 minutes using a DIN 4188 sieve with an aperture of 0.255 mm.

Green ceramic bodies were prepared by cold uniaxial pressing using a SKAY press with a capacity of 30 tons. The ceramic discs were prepared molds with a diameter of 20 mm for the purpose of Archimedes tests before being pressed over two stages. The first stage involved a preload of 15 MPa for 30 seconds to settle the powders in the mold, while the second involved pressing with a load of 50 MPa to compress the powders and form a pellet.

Sintering of the samples was carried out conventionally in the absence of a controlled atmosphere. A JUNG furnace was used in which a maximum temperature of 1400 °C was reached. The sintering route is shown in *Figure 1*.

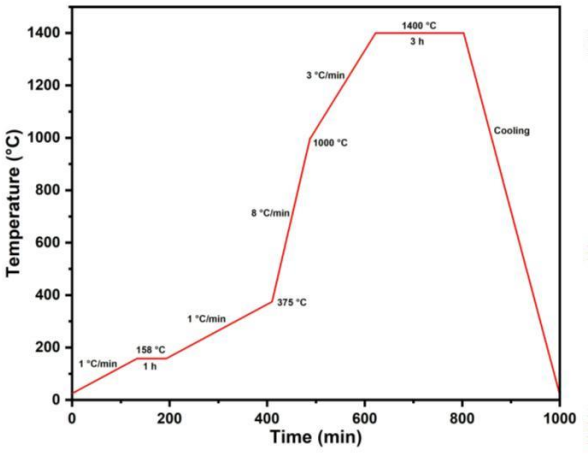

Figure 1: Sintering ramp adopted in this study

Table 3: Density and green densification results of the ceramic green bodies

Sample mixture	Density (g/cm^3)	Relative Density (%)
Al_2O_3-Nb_2O_5	2.02 ± 0.01	50.64 ± 0.44
Al_2O_3-Nb_2O_5-LiF	2.12 ± 0.10	53.37 ± 2.57
Al_2O_3-TiC-Nb_2O_5	1.48 ± 0.05	33.86 ± 1.21
Al_2O_3-TiC-Nb_2O_5-LiF	1.44 ± 0.10	33.11 ± 2.31

2.3. Characterization

Density of green bodies

From the theoretical density value obtained using the Rule of Mixtures, it was possible to calculate the density and densification of the ceramic bodies in the initial production phase. *Equation 2* was used to determine the density of the bodies (ρ_{gb}) in the initial phase by dividing the mass of the sample (m_{sample}) by its volume (v_{sample}).

$$\rho_{gb} = \frac{m_{sample}}{v_{sample}} \quad (2)$$

Densification in the initial phase was calculated by *Equation 3* based on the percentage difference between the obtained density (ρ_{gb}) and theoretical density (ρ_{theo}) values using the Rule of Mixtures.

$$\%TD = \frac{\rho_{gb}}{\rho_{theo}} \cdot 100\% \quad (3)$$

Density of sintered samples

The density and densification of the sintered ceramic bodies were calculated based on the standard ABNT NBR 16667:2017 [26]. The calculation is based on the Archimedes' principle using the data of immersed mass (m_i), wet mass (m_w) and dry mass (m_d) to determine the apparent density according to *Equation 4*:

$$\rho_{apparent} = \left(\frac{m_d}{m_w - m_i}\right) \quad (4)$$

During the analysis, a beaker containing deionized water was heated up to its boiling point before the samples were placed in this boiling water for 1h to remove any impurities. Afterwards, the samples were weighed, and their initial mass m_i recorded before carefully removing the excess moisture from the samples using paper and measuring their mass m_w. Subsequently, the samples were dried in an oven at 120 °C for 2h to remove all the moisture in the sintered samples, thereby enabling their mass m_d to be measured. From the masses obtained, it was possible to determine the relative density of the ceramic bodies by calculating the difference between the apparent and theoretical densities of each composition (*Equation 5*).

$$Relative\ Density = \left(\frac{\rho_{apparent}}{\rho_{theo}}\right) \cdot 100\% \quad (5)$$

Scanning Electron Microscopy (SEM)

The fracture surface of the sintered samples was analyzed using a Quanta FEG-250 scanning electron microscope. Beam power settings of 5, 20 and 25 kV were used with a beam diameter of 5.5 µm as well as magnifications of 500x and 2000x to observe the microstructures. The samples were coated with gold to enable visualization by the SEM.

3. Results and discussion

3.1. Density of the green bodies

The density and green densification values of the four sample mixtures before sintering are presented in *Table 3*.

Based on the values displayed in *Table 3*, it was observed that the samples to which TiC was not added yielded satisfactory results regarding green densification. It is important to emphasize that in order for ceramics to achieve satisfactory levels of densification after sintering, the green bodies need to achieve a relative density of between approximately 55 and 65% of the theoretical density. However, the samples to which TiC was added exhibited very low densification values, resulting in an unsatisfactory degree of densification of the bodies after sintering.

Furthermore, another factor that must be considered is how difficult it was to press the bodies to which TiC was added due to the presence of lamination and end-capping defects. The high concentration of TiC used led to an insufficient level of homogenization, impairing densification of the green bodies.

3.2. Density of the sintered samples

In *Table 4*, the density and densification values of the sintered ceramic composites are displayed.

Significant discrepancies were observed between the average densification values of the different sample mixtures. In the Al_2O_3-Nb_2O_5-LiF sample mixture, the highest degree of densification was observed compared to the other groups with values close to those obtained in the literature, that is, in excess of 91% of the theoretical density [11-12, 18]. On the other hand, the Al_2O_3-Nb_2O_5 sample mixture exhibited a lower degree of densification, namely approximately 85% of the theoretical density,

Table 4: Density and densification results of the sintered ceramics

Sample mixture	Density (g/cm^3)	Relative Density (%)
Al_2O_3-Nb_2O_5	3.39 ± 0.07	84.88 ± 1.77
Al_2O_3-Nb_2O_5-LiF	3.69 ± 0.02	92.71 ± 0.50
Al_2O_3-TiC-Nb_2O_5	1.06 ± 0.01	24.22 ± 0.26
Al_2O_3-TiC-Nb_2O_5-LiF	1.27 ± 0.01	29.19 ±0.58

due to the formation of only the $AlNbO_4$ phase during homogenization [27]. Meanwhile, the sample mixture containing LiF and Nb_2O_5 showed interaction between these two compounds, resulting in the formation of the $LiNbO_3$ and Nb_3O_7F phases during sintering [28].

In turn, the two groups containing TiC in the composition presented severe reductions in sample densification, with values below 30% of the theoretical density. This low densification can be attributed to the high content of TiC used in the composition (38.5 wt.%), which prevents accommodation of the material as an interstitial element in alumina.

Based on data in the literature, it is possible to assume that in the absence of an inert atmosphere, TiC reacts with oxygen, forming TiO_2, which could promote sintering in the presence of a liquid phase [23],[25]. However, the excessively high concentration of TiC, combined with the low level of densification of the ceramic discs during pressing, may have hindered interaction between the samples, resulting in porous and brittle discs.

3.3. Microstructure analysis

The fracture surfaces of the sintered samples obtained by SEM at different magnifications are illustrated in *Figures 2* and *3*.

The micrographs in *Figure 2* generally depict the fracture region of the sintered samples. It can be observed that the samples from the Al_2O_3-Nb_2O_5 and Al_2O_3-Nb_2O_5-LiF sample mixtures exhibit lower surface porosity, given the high densification achieved during the sintering process in these two sample mixtures.

On the other hand, the samples to which TiC was added exhibited high degrees of porosity on their surfaces due to low grain interaction during the sintering process. When the samples were coated before SEM analysis, it was difficult to deposit gold on the TiC samples, as some of the material was deposited in the pores and therefore, removed from the surface. Consequently, it was not possible to generate images of these two samples mixtures with the same electron beam power (25 kV) during the analysis. The beam power had to be reduced to 5 kV for the analysis of the Al_2O_3-TiC-Nb_2O_5 sample mixture due to excessive light charging in the image, moreover, a beam power of 20 kV was used for the sample mixture containing Al_2O_3-TiC-Nb_2O_5-LiF.

Micrographs magnified at 2000x to improve the visualization of grain morphology are presented in *Figure 3*.

The micrographs in *Figure 3* provide a more detailed insight into the grain morphology. The Al_2O_3-Nb_2O_5 and Al_2O_3-Nb_2O_5-LiF sample mixtures exhibit rounded grains with well-defined necks, indicating good degrees of compaction and sintering. Although some pores are present, they are small and uniformly distributed throughout the sample mixtures as a result of effective wetting of the liquid phase during sintering.

On the other hand, the two sample mixtures to which TiC was added, that is Al_2O_3-TiC-Nb_2O_5 and Al_2O_3-TiC-Nb_2O_5-LiF contain a significant number of

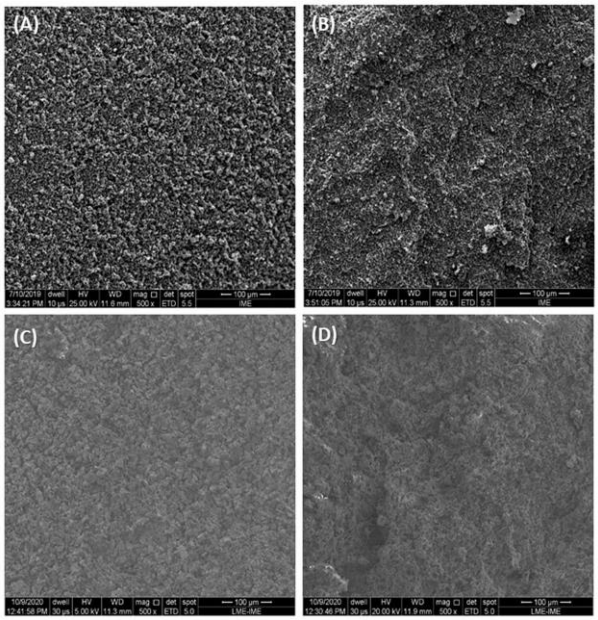

Figure 2: Fracture region micrographs of the sintered samples with a magnification of 500x
(a) Al_2O_3-Nb_2O_5; (b) Al_2O_3-Nb_2O_5-LiF;
(c) Al_2O_3-TiC-Nb_2O_5; (d) Al_2O_3-TiC-Nb_2O_5-LiF

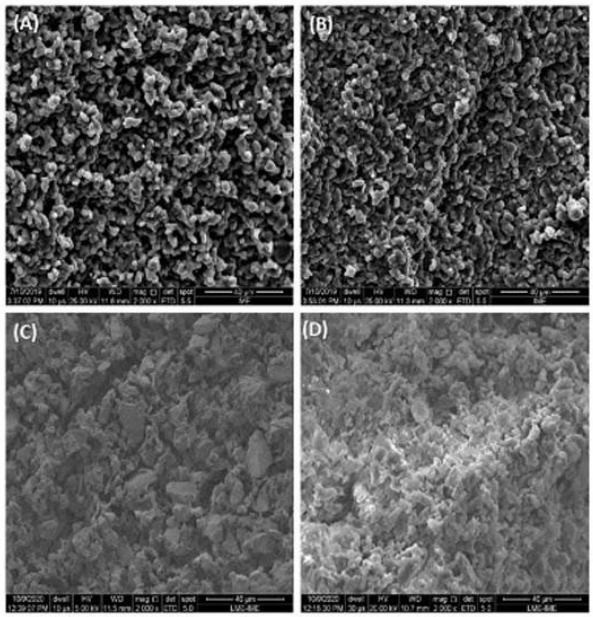

Figure 3: Micrographs of the fracture regions of the sintered samples under 2000x magnification
(a) Al_2O_3-Nb_2O_5; (b) Al_2O_3-Nb_2O_5-LiF;
(c) Al_2O_3-TiC-Nb_2O_5; (d) Al_2O_3-TiC-Nb_2O_5-LiF

pores and grains of various sizes. This could be attributed to poor homogenization during grinding, leading to difficulties in compaction and sintering of the sample mixtures, ultimately resulting in a depleted microstructure.

Regarding the ballistic applications of Al_2O_3–TiC ceramics, in light of the possible addition of Nb_2O_5 and LiF, a wide range of parameters must be investigated to obtain dense and very hard ceramics capable of withstanding ballistic impacts. These parameters include

temperature, composition and cold uniaxial pressing load amongst other factors.

To date, Al_2O_3 ceramics to which TiC was added have not been applicable due to their low degree of densification. However, samples to which TiC was not added exhibit high levels of densification and have been reported to possess good ballistic properties [12].

It is worth noting that these ceramics are also applied in other areas such as in cutting tools [29], substrates [30], high-temperature electromagnetic applications [31] and abrasives [32] amongst various others. The development and optimization of these materials would make it possible for the performance across different industries and technological sectors to be significantly improved.

4. Conclusions

In this study, four distinct sample mixtures of ceramic matrix composites were produced by cold uniaxial pressing and conventional sintering. These sample mixtures were subsequently characterized using the Archimedes' principle and scanning electron microscopy (SEM). Based on the obtained results, it can be concluded that the samples to which TiC was added exhibited low initial densities, indicating that the pressure of 50 MPa was insufficient to achieve an adequate level of densification of the green bodies. Furthermore, the presence of TiC drastically reduced the degree of densification, making the application of a conductive coating for SEM analysis challenging and necessitating adjustments to the electron beam intensity for the analysis to be made. On the other hand, the sample mixtures to which TiC was not added exhibited high density values in the green state, moreover, after sintering, yielded results consistent with previous research, indicating a satisfactory level of sintering in the absence of TiC.

Acknowledgements

This study was financed in part by the Coordenação de Aperfeiçoamento de Pessoal de Nível Superior – Brasil (CAPES) – Finance Code 001.

REFERENCES

[1] Gerlei, V.; Kránicz, T.; Korim, T.; Jakab, M.: Manufacturing of large and polished ceramic pistons by cold isostatic pressing, *Hung. J. Ind. Chem.*, 2023, **51**(1), 29–34, DOI: 10.33927/hjic-2023-05

[2] Wisdom, A.; Mark, U.; Zeberu, E.; Adeleke, A.: Optimisation of the physical properties of rice husk ash in ceramic materials using the response surface methodology, *Hung. J. Ind. Chem.*, 2021, **49**(1), 23–30, DOI: 10.33927/hjic-2021-04

[3] Tepeduzu, B.; Karakuzu, R.: Ballistic performance of ceramic/composite structures, *Ceram. Int.*, 2019, **45**(2), 1651–1660, DOI: 10.1016/j.ceramint.2018.10.042

[4] Ribeiro, M.P.; Neuba, L.d.M.; da Silveira, P.H.P.M.; da Luz, F.S.; Figueiredo, A.B.-H.d.S.; Monteiro, S.N.; Moreira, M.O.: Mechanical, thermal and ballistic performance of epoxy composites reinforced with *Cannabis sativa* hemp fabric, *J. Mater. Res. Technol.*, 2021, **12**, 221–233, DOI: 10.1016/j.jmrt.2021.02.064

[5] Cardoso, B.F.d.A.F.; Ramos, F.J.H.T.V.; da Silveira, P.H.P.M.; Figueiredo, A.B.-H.d.S.; Gomes, A.V.; da Veiga-Junior, V.F.: Mechanical and ballistic characterization of high-density polyethylene composites reinforced with alumina and silicon carbide particles, *J. Met. Mater. Miner.*, 2022, **32**(2), 42–49, DOI: 10.55713/jmmm.v32i2.1262

[6] da Silva, T.T.; da Silveira, P.H.P.M.; Figueiredo, A.B.-H.d.S.; Monteiro, S.N.; Ribeiro, M.P.; Neuba, L.d.M.; Simonassi, N.T.; Garcia Filho, F.d.C.; Nascimento, L.F.C.: Dynamic mechanical analysis and ballistic performance of kenaf fiber-reinforced epoxy composites, *Polymers*, 2022, **14**(17), 3629, DOI: 10.3390/polym14173629

[7] Silva, M.V.; Stainer, D.; Al-Qureshi, H.A.; Montedo, O.R.K.; Hotza, D.: Alumina-based ceramics for armor application: Mechanical characterization and ballistic testing, *J. Ceram.*, 2014, **2014**, 618154, DOI: 10.1155/2014/618154

[8] Karandikar, P.G.; Evans, G.; Wong, S.; Aghajanian, M.K.; Sennett, M.: Chapter 16 - A review of ceramics for armor applications, in: Advances in ceramic armor IV: Ceramic engineering and science proceedings, Prokurat Franks, L. (Ed), 2009, **29**(6), pp. 163–175, DOI: 10.1002/9780470456286.ch16

[9] da Silveira, P.H.P.M.; da Silva, T.T.; Ribeiro, M.P.; de Jesus, P.R.R.; Credmann, P.C.R.d.S.; Gomes, A.V.: A brief review of alumina, silicon carbide and boron carbide ceramic materials for ballistic applications, *Acad. Lett.*, 2021, 3742, DOI: 10.20935/AL3742

[10] Yadav, S.; Ravichandran, G.: Penetration resistance of laminated ceramic/polymer structures, *Int. J. Impact Eng.*, 2003, **28**(5), 557–574, DOI: 10.1016/S0734-743X(02)00122-7

[11] Santos, J.l.; Marçal, R.L.S.B.; Jesus, P.R.R.; Gomes, A.V.; Lima Jr., E.P.; Monteiro, S.N.; de Campos, J.B.; Louro, L.H.L.: Effect of LiF as sintering agent on the densification and phase formation in Al_2O_3-4 wt pct Nb_2O_5 ceramic compound, *Metall. Mater. Trans. A*, 2017, **48**(10), 4432–4440, DOI: 10.1007/s11661-017-4271-y

[12] dos Santos, J.L.; Marçal, R.L.S.B.; de Jesus, P.R.R.; Gomes, A.V.; Lima Jr, E.P.; da Rocha, D.N.; dos Santos, M.A.P.; Nascimento, L.F.C.; Monteiro, S.N.; Louro, L.H.L.: Mechanical properties and ballistic behavior of LiF-added Al_2O_3–4wt% Nb_2O_5 ceramics, *J. Mater. Res. Technol.*, 2018, **7**(4), 592–597, DOI: 10.1016/j.jmrt.2018.09.005

[13] Seong, W.-K.; Ahn, B.-M.; Min, Y.; Hwang, G.-T.; Choi, J.-J.; Choi, J.-H.; Hahn, B.-D.; Cho, Y.-R.; Ahn, C.-W.: Effect of Nb_2O_5 addition on microstructure and thermal/mechanical properties in zirconia-toughened alumina sintered at low temperature, *Ceram. Int.*, 2020, **46**(15), 23820–23827, DOI: 10.1016/j.ceramint.2020.06.158

[14] Huang, C.-Y.; Chen, Y.-L.: Effect of mechanical properties on the ballistic resistance capability of Al_2O_3-ZrO_2 functionally graded materials, *Ceram. Int.*, 2016, **42**(11), 12946–12955, DOI: 10.1016/j.ceramint.2016.05.067

[15] Boldin, M.S.; Berendeev, N.N.; Melekhin, N.V.; Popov, A.A.; Nokhrin, A.V.; Chuvildeev, V.N.: Review of ballistic performance of alumina: Comparison of alumina with silicon carbide and boron carbide, *Ceram. Int.*, 2021, **47**(18), 25201–25213, DOI: 10.1016/j.ceramint.2021.06.066

[16] Dresch, A.B.; Venturini, J.; Arcaro, S.; Montedo, O.R.K.; Bergmann, C.P.: Ballistic ceramics and analysis of their mechanical properties for armour applications: A review, *Ceram. Int.*, 2021, **47**(7), 8743–8761, DOI: 10.1016/j.ceramint.2020.12.095

[17] Fabris, D.C.N.; Polla, M.B.; Acordi, J.; Luza, A.L.; Bernardin, A.M.; De Noni Jr, A.; Montedo, O.R.K.: Effect of $MgO{\cdot}Al_2O_3{\cdot}SiO_2$ glass-ceramic as sintering aid on properties of alumina armors, *Mater. Sci. Eng. A*, 2020, **781**, 139237, DOI: 10.1016/j.msea.2020.139237

[18] da Silveira, P.H.P.M.; de Jesus, P.R.R.; Ribeiro, M.P.; Monteiro, S.N.; De Oliveira, J.C.S.; Gomes, A.V.: Sintering behavior of Al_2O_3 ceramics doped with pre-sintered NB_2O_5 and LiF, *Mater. Sci. Forum*, 2020, **1012**, 190–195, DOI: 10.4028/www.scientific.net/MSF.1012.190

[19] Cabral, R.F.; Prado da Silva, M.H.; de Campos, J.B.; Lima, E.S.: Study of the sintering of mixtures Al_2O_3-Nb_2O_5 and Y_2O_3-Nb_2O_5, *Mater. Sci. Forum*, 2012, **727-728**, 799–803, DOI: 10.4028/www.scientific.net/MSF.727-728.799

[20] Fu, Z.; Koc, R.: Pressureless sintering of submicron titanium carbide powders, *Ceram. Int.*, 2017, **43**(18), 17233–17237, DOI: 10.1016/j.ceramint.2017.09.050

[21] Compton, B.G.;, Zok, F.W.: Impact resistance of TiC-based cermets, *Int. J. Impact Eng.*, 2013, **62**, 75–87, DOI: 10.1016/j.ijimpeng.2013.06.008

[22] Cheng, L.; Xie, Z.; Liu, G.; Liu, W.; Xue, W.: Densification and mechanical properties of TiC by SPS-effects of holding time, sintering temperature and pressure condition, *J. Eur. Ceram. Soc.*, 2012, **32**(12), 3399–3406, DOI: 10.1016/j.jeurceramsoc.2012.04.017

[23] Koc, R.; Folmer, J.S.: Carbothermal synthesis of titanium carbide using ultrafine titania powders, *J. Mater. Sci.*, 1997, **32**(12), 3101–3111, DOI: 10.1023/A:1018634214088

[24] Mhadhbi, M.; Driss, M.: Titanium carbide: synthesis, properties and applications, *J. Brill. Eng. (BEN)*, 2021, **2**(2), 1–11, DOI: 10.36937/ben.2021.002.001

[25] Koc, R.: Kinetics and phase evolution during carbothermal synthesis of titanium carbide from carbon-coated titania powder, *J. Eur. Ceram. Soc.*, 1997, **17**(11), 1309–1315, DOI: 10.1016/S0955-2219(96)00241-5

[26] Associação Brasileira de Normas Técnicas, Rio de Janeiro: NBR 16661, 2017

[27] Kong, F.; Lv, L.; Wang, J.; Jiao, G.; Tao, S.; Han, Z.; Fang, Y.; Qian, B.; Jiang, X.: Graphite modified $AlNbO_4$ with enhanced lithium – Ion storage behaviors and its electrochemical mechanism, *Mater. Res. Bull.*, 2018, **97**, 405–410, DOI: 10.1016/j.materresbull.2017.09.034

[28] Huang, F.; Zhao, H.; Yan, A.; Li, Z.; Liang, H.; Gao, Q.; Qiang, Y.: *In situ* thermal decomposition for preparation of Nb_3O_7F/Nb_2O_5 hybrid nanomaterials with enhanced photocatalytic performance, *J. Alloys Compd.*, 2017, **695**, 489–495, DOI: 10.1016/j.jallcom.2016.11.113

[29] Grigoriev, S.N.; Nadykto, A.B.; Volosova, M.A.; Zelensky, A.A.; Pivkin, P.M.: WEDM as a replacement for grinding in machining ceramic Al_2O_3-TiC cutting inserts, *Metals*, 2021, **11**(6), 882, DOI: 10.3390/met11060882

[30] Liu, C.; Sun, J.; Venturi, F.; Romero, A.R.; Hussain, T.: Microstructure and wear performance of alumina/graphene coating on textured Al_2O_3/TiC substrate composites, *J. Eur. Ceram. Soc.*, 2021, **41**(2), 1438–1451, DOI: 10.1016/j.jeurceramsoc.2020.09.063

[31] Shao, T.; Ma, H.; Wang, J.; Feng, M.; Yan, M.; Wang, J.; Yang, Z.; Zhou, Q.; Luo, H.; Qu, S.: High temperature absorbing coatings with excellent performance combined Al_2O_3 and TiC material, *J. Eur. Ceram. Soc.*, 2020, **40**(5), 2013–2019, DOI: 10.1016/j.jeurceramsoc.2020.01.036

[32] Grigoriev, S.N.; Volosova, M.A.; Okunkova, A.A.; Fedorov, S.V.: Influence of defects in surface layer of Al_2O_3/TiC and SiAlON ceramics on physical and mechanical characteristics, *Ceramics*, 2023, **6**(2), 818–836, DOI: 10.3390/ceramics6020047